DOI: 10.1002/ejic.200700991

The Synthesis of Multiwalled Rare-Earth Phosphate Nanomaterials Using Organophosphates with Upconversion Properties

Hua Li,[a] Guangshan Zhu,*[a] Hao Ren,[a] Yi Li,[a] Ian J. Hewitt,[a] and Shilun Qiu*[a]

Keywords: Microporous materials / Organophosphonates / Nanomaterials / Rare earths

Tributylphosphate, an organophosphate, was used as the phosphorus source instead of phosphoric acid to synthesize several new multiwalled, microporous rare-earth phosphate nanofibers and nanotubes.

Introduction

Since the discovery of carbon nanotubes in 1991,[1] one-dimensional (1D) nanostructured materials such as nanowires, nanobelts, nanotubes, and nanorods sparked worldwide interest because of their unique electronic, optical, and mechanical properties with respect to the corresponding bulk materials. These materials have subsequently found numerous potential applications.[2] By restricting the growth to one dimension, it is possible to influence the optical, magnetic, and electronic properties of the products. Metal phosphates have been widely utilized in nonlinear optical materials, phosphors, sensors, heat-resistant, biocompatible materials, materials used for catalysis and separation, as well as in environmental and advanced functional materials.[3–6] In particular, materials with functional metal centers, rare-earth or rare-earth-doped phosphate materials, have received intense attention because of their special coordination properties and ability to form isostructural complexes with fantastic physical and chemical characteristics.[7] They have extensive applications in many chemical processes and photonic devices due to the position of their 4f electrons, which are well shielded from the effects of the neighboring ions.[8] The lanthanide phosphate nanomaterials synthesized to date mostly have a dense structure due to the strong affinity of the phosphate group toward lanthanide elements and exhibit interesting optical or magnetic properties.[9] The synthesis of these compounds is generally carried out under hydrothermal conditions by using a metal salt and phosphoric acid. The high coordination number and flexible coordination geometry of lanthanide metal ions make it difficult to control the porosity of lanthanide complexes. In order to obtain microporous lanthanide compounds, phosphate anions have been substituted by other chelating agents, which prevent the formation of dense, insoluble inorganic species, or bridging ligands have been incorporated with the desired size and shape.[10] The first rare-earth phosphate nanotubes made of $CePO_4$ have been reported recently, and they are promising candidates for some optical devices.[11] However, the formation of rare-earth phosphate porous materials by using organic templates still remains a challenge.

Near-infrared-to-visible upconversion has been an important approach for the generation of visible luminescence and short-wavelength lasers.[12] The use of upconversion phosphors (UCPs) as fluorescent labels in the sensitive detection of biomolecules has attracted greater interest lately.[13] In comparison with downconversion phosphors, such as dyes, UCP fluorescent labels have very low levels of background noise, and near-infrared light is less harmful to the human body than UV light. However, as luminescent biological labels, especially for the sensitive analysis of molecules such as DNA, RNA, or proteins, nanosized UCPs are required.[14–15] At the nanoscale, rare-earth phosphates show improved properties, for example, enhanced optical, magnetic, and catalytic properties, because energy can be transferred to rare-earth ions more effectively in this scale.[16] In environmental detection, upconversion can also find application in infrared detection by converting the invisible light into the visible range for orientation, etc.

Herein, we report a simple hydrothermal method to produce multiwalled rare-earth phosphate nanomaterials with microporous properties by using an organophosphate instead of H_3PO_4 as the phosphate source. The thermal stability, water sorption, and luminescent properties have been

[a] State Key Laboratory of Inorganic Synthesis & Preparative Chemistry, Jilin University,
Changchun 130012, China
Fax: +86-431-85168331
E-mail: zhugs@mail.jlu.edu.cn
sqiu@mail.jlu.edu.cn

Supporting information for this article is available on the WWW under http://www.eurjic.org or from the author.

investigated. These nanosized hollow fibers and tubes with layered structure show adsorption behavior that favors H_2O uptake. In addition, they exhibit strong fluorescence in the visible region, and $ErPO_4$ shows characteristic upconversion green emission due to Er^{3+} at room temperature. The fluorescent intensity of these nanomaterials is much stronger than that of the corresponding bulk materials. These nanomaterials could be anticipated to have applications as fluorescent materials, and $ErPO_4$ could be a good upconversion emitter.

Results and Discussion

X-ray diffraction measurements (Figure 1) indicate that the $LnPO_4$ materials display crystalline structures that are different from those of the traditional rare-earth phosphates. The powder X-ray diffraction patterns of the as-synthesized materials are not consistent with those of the corresponding rare-earth phosphates reported in the literature.[9] The one notable difference is the very intense peak located at the low Bragg angle 2θ of 6.82° ($d \approx 1$ nm), indicating the possible formation of a newly organized structure due to the assembly of nanostructured materials. The pattern was indexed with a hexagonal unit cell [a = 15.0359(5) Å, c = 9.998(1) Å, V = 1957.43 Å^3, $M(20)$ = 127,[17] $F(20)$ = 183[18]] with the program TREOR (index software).[19] The peaks of all the samples are broader, implying smaller crystallinity. Powder X-ray diffraction performed on all the samples reveals that they are identical in structure and have the same general formula (Scheme 1). Thus, we will restrict our presentation and discussion to the erbium phosphate.

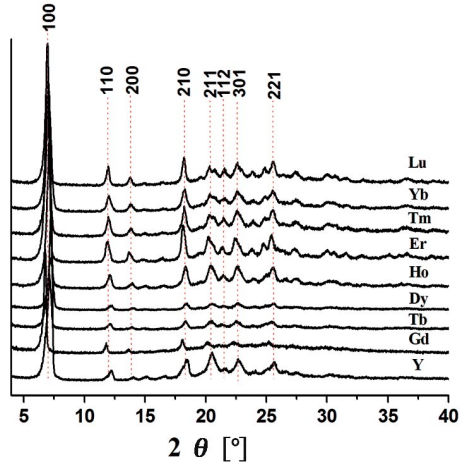

Figure 1. The XRD patterns of $LnPO_4$.

For some lanthanide compounds, the morphology of the product appears to be dependent on the reaction concentration. When the reaction proceeds at low concentration, uniform nanofibers are formed as observed by using SEM and optical microscopy (Figure 2). Optically, the fibers appear uniform and transparent (Figure 2 top left). High-magnification SEM images of the fibers (Figure 2 middle) show that they bundle together and each bundle has a width of 70–100 nm. This fibrous structure was found to occur for each of the lanthanide compounds studied. When the synthesis was repeated at higher concentration with Er, Y, or Tb, the formation of nanotubes was observed (Figure 2 bottom) although a small amount of nanofibers was still found to be present. The appearance and dimensionality of the nanotubes was observed to be similar to that of the nanofibers with a 2 nm cavity.

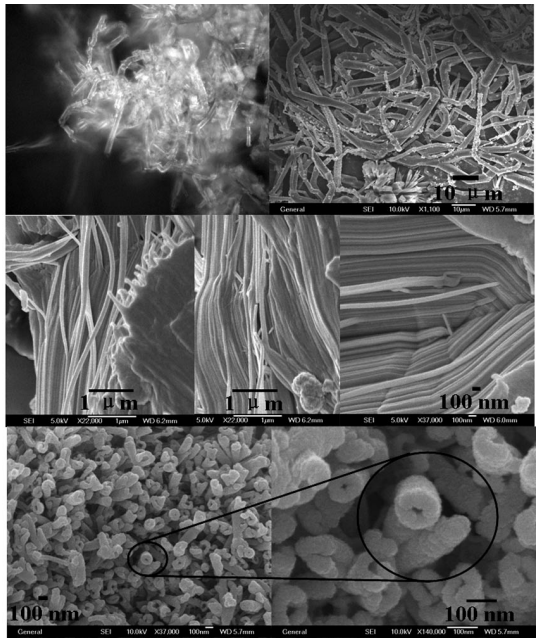

Figure 2. Top: reflected-light optical microscope images (left) and SEM images (right) of the nanofiber bundles; middle: magnified images of the nanofibers; bottom: top view of SEM images of nanotubes, at low (left) and high (right) magnification.

Further insights into the details of the morphology and microstructure were obtained from TEM images (Figure 3). From the preferred orientation of the fibers (Figure 3a–c), it can be observed that the linear microstructures are parallel to the long axis of the fibers, which is consistent with XRD results. For both nanotubes and nanofibers, lattice fringes with ca. 1 nm spacing are observed. This distance

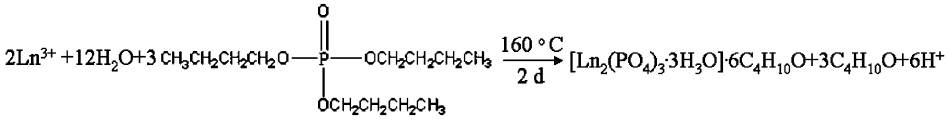

Scheme 1.

of ca. 10 Å is very close to the *d* spacing of the broad peaks at $2\theta = 6.8°$ in the XRD pattern, and, as previously mentioned, the observed spectra are quite different from those of the bulk phase of $LnPO_4$.

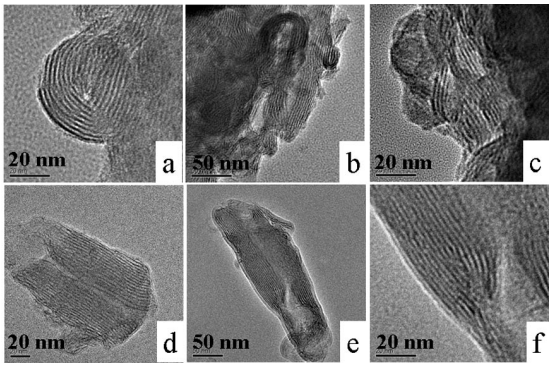

Figure 3. TEM images of the nanofibers (a), (b), (c) and the nanotubes (d), (e), (f).

The formation of layered structure materials during hydrothermal synthesis is a complex process. The mechanism of nucleation and growth is a little difficult to elucidate. Since no organic amine base was added to the solution, we suggest that the butanol molecules formed during the hydrolysis of the phosphate act as the template. We also propose that, because of the insoluble nature of butyl phosphate in water at room temperature, the slow release of PO_4^{3-} results in the formation of multiwalled materials that are different from the other $LnPO_4$ compounds that have been reported.[9] The butanol molecules formed in high concentration as a result of the hydrolysis of the organophosphate during the reaction often form a double-layered arrangement, and these butanol double layers play the role of templates for the formation of inorganic layers through hydrogen-bond interactions between the hydroxy and phosphate groups. The growth of the nanotube may occur in stages, starting with a radial self-organized arrangement of lamina followed by the rolling of the lamina into nanotubes (Figure S3b). This stepwise growth mechanism may enable the formation of this new type of rare-earth phosphate nanostructure.

Thermogravimetric analysis (TGA) of the Er compound (Figure S1) showed that the first weight loss of 31.7% from 100 to 300 °C corresponds to the partial loss of butanol molecules. The second weight loss of 16.3% from 300 to 450 °C corresponds to the loss of the rest of the butanol molecules and the accompanying decomposition. The composition of the as-made product was determined as $[Ln_2(PO_4)_3{\cdot}3H_3O]{\cdot}6[C_4H_{10}O]$ on the basis of elemental (C 33.14, H 6.57, Er 53.9, P 15.1) and TG analyses. This formula suggests that the butanol molecules interact with and become incorporated into the rare-earth phosphate nanostructure.

The observation of multiwalled frameworks and thermal stability encouraged us to try to create micropores after calcination. The compound after calcination at 300 °C was evacuated under reduced pressure (1×10^{-5} Torr) until there was no more weight loss at 150 °C, and then the dehydrated sample was exposed to water vapor. As shown in Figure S2, type I behavior in the range $P/P_0 = 0$–0.5 is observed for the water adsorption isotherm of the sample, which is characteristic of solids with micropores. At the saturation point, the amount of water sorbed is 64.5 mg g^{-1}, which is equivalent to the adsorption of about 3.5 H_2O molecules per formula unit. Therefore, the pore volume after calcination at 300 °C is estimated to be approximately 0.07 mL g^{-1} from the water adsorption isotherm. A second augmentation of the amounts sorbed in the range $P/P_0 > 0.5$ can be attributed to adsorption on the external crystallite surface.[15] It is, however, a pity that we have not been able to obtain the N_2 absorption isotherm; this may be because butanol molecules acting as the template in the microstructures cannot be completely removed from the negatively charged framework (Figure S3).

The downconversion emission and excitation spectra of the Er sample are shown in Figure 4. Upon UV excitation ($\lambda = 235$ nm), $ErPO_4$ nanomaterials exhibit strong green luminescence caused by f–f transitions in the erbium ions. The main emission bands at 523 and 557 nm are associated with the $^2H_{11/2} \rightarrow {}^4I_{15/2}$ and $^4S_{3/2} \rightarrow {}^4I_{15/2}$ transitions of the Er^{3+} ions, respectively.[20] In comparison with bulk $ErPO_4$ material, the nanomaterial exhibited much stronger fluorescence under the same measurement conditions.

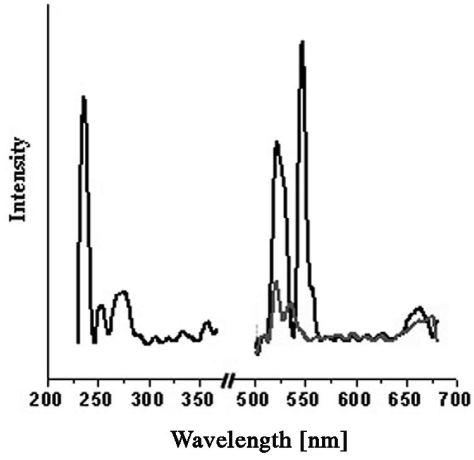

Figure 4. Downconversion emission and excitation spectra of the erbium phosphate nanostructure (the gray curve is for the bulk material).

Continuous-wave excitation with a 980-nm IR laser at room temperature leads to the upconversion emission of the Er^{3+} nanomaterial in the visible region, as shown in Figure 5 along with the energy level diagram of the Er^{3+} ions.[21] The peaks were assigned to the following transitions: the green emission in the 520–570 nm region is assigned to the $(^2H_{11/2}, {}^4S_{3/2}) \rightarrow {}^4I_{15/2}$ transition, and the red emission in the 650–670 nm region is assigned to the $^4F_{9/2} \rightarrow {}^4I_{15/2}$ transition for the Er^{3+} ion. The upconversion mechanism corresponding to green and red emissions can be described by a two-photon process.[20]

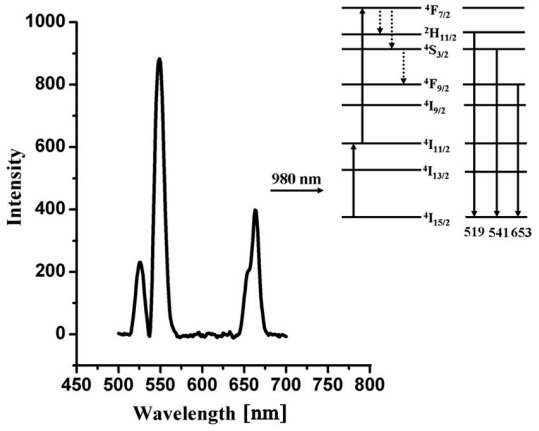

Figure 5. Upconversion emission spectrum of the erbium phosphate material (the inset is the energy level diagram of the Er^{3+} ions) obtained by pumping with a 980-nm laser.

Conclusions

In summary, a series of microporous rare-earth phosphates have been synthesized by reaction of Ln^{3+} with PO_4^{3-}, which hydrolyzed slowly from butyl phosphate in a mixed water solution by facile hydrothermal treatment. The use of the phosphate ester influences the release of phosphate ions in the solution, thereby affecting the course of the reaction and the products formed. Powder X-ray diffraction analyses reveal that the products are extremely similar in structure. The water sorption isotherm proves that most guest molecules in the framework of the complex can be removed to create permanent microporosity. Upon UV excitation, the characteristic luminescence from f–f transitions is observed. The green and red upconversion emissions were observed under excitation by 980-nm radiation. Such nanofibers and nanotubes have a variety of promising applications. Furthermore, the properties exhibited by these novel functional materials will find potential application in various fields.

Further work is under way to study the formation mechanism and detailed properties of this novel morphology and to investigate the possibility of synthesizing other nanomaterials such as doped materials and achieving complete removal of the organic template from the micropores.

Experimental Section

General Remarks: All chemicals purchased were of reagent grade or better and were used without further purification. Rare-earth nitrate salts were prepared by dissolving rare-earth oxides with HNO_3 (6 M), followed by the addition of some H_2O_2 for Tb_4O_7, then concentration at 100 °C until the crystal film formed. The XRD was performed with a Siemens D5005 diffractometer using Cu-K_α radiation, 40 kV, 35 mA with a scanning rate of 0.3°min^{-1} (2θ). The SEM image was recorded with a JEOL JSM-6700F scanning electron microscope and Iridium (IXRF Systems) software. The elemental analyses were carried out with a Perkin–Elmer 240C elemental analyzer. Thermal gravimetric analyses (TGA) were performed under nitrogen with a heating rate of 10 °C min^{-1} by using a Perkin–Elmer TGA 7 thermogravimetric analyzer. Fluorescence spectroscopy data were recorded with a LS55 luminescence spectrometer. Water sorption isotherms were obtained by measuring the increase in weight at equilibrium as a function of relative pressure. The weight of sample was measured by a CAHN 2000 electrobalance and the adsorbate (H_2O) was added incrementally and manually.

Synthesis of $[Er_2(PO_4)_3{\cdot}3H_3O]{\cdot}6[C_4H_{10}O]$: A mixture of butyl phosphate (0.25n mmol) and $Er(NO_3)_3{\cdot}6H_2O$ (0.25n mmol) (n = 0.5–3) was suspended in deionized water (10 mL) at room temperature. The clear mixture (pH ≈ 5–6) was sealed in a 15-mL Teflon-lined autoclave after stirring for 60 min. After being heated at 160 °C for 2 d, the autoclave was naturally cooled to room temperature. Following ultrasonic washing, the samples were thoroughly washed with distilled water, filtered, and dried at room temperature. Synthesis of the other rare-earth phosphates was carried out with the same procedure except that erbium was replaced by Y, Gd, Tb, Dy, Ho, Tm, Yb, and Lu.

Supporting Information (see footnote on the first page of this article): TGA curves, water sorption isotherm and pictorial representation of the growth mechanism hypothesized in this paper.

Acknowledgments

This work was funded by the State Basic Research Project (No. G2000077507) and the National Nature Science Foundation of China (Grant no. 29873017, 20273026, and 20101004).

[1] S. Iijima, *Nature* **1991**, *354*, 56–58.
[2] a) J. Hu, M. Ouyang, P. Yang, C. M. Lieber, *Nature* **1999**, *399*, 48–51; b) J. Hu, T. W. Odom, C. M. Lieber, *Acc. Chem. Res.* **1999**, *32*, 435–445; c) F. Favier, E. C. Walter, M. P. Zach, T. Benter, R. M. Penner, *Science* **2001**, *293*, 2227–2231; d) W. Tremel, *Angew. Chem.* **1999**, *111*, 2311–2315; *Angew. Chem. Int. Ed.* **1999**, *38*, 2175–2179.
[3] a) A. K. Cheetham, G. Férey, T. Loiseau, *Angew. Chem. Int. Ed.* **1999**, *38*, 3268–3292.
[4] C. N. R. Rao, S. Natarajan, A. Choudhury, S. Neeraj, A. A. Ayi, *Acc. Chem. Res.* **2001**, *34*, 80–87.
[5] J. Yu, R. Xu, *Acc. Chem. Res.* **2003**, *36*, 481–490.
[6] Z. Yin, Y. Sakamoto, J. Yu, S. Sun, O. Terasaki, R. Xu, *J. Am. Chem. Soc.* **2004**, *126*, 8882–8883.
[7] a) A. Thirumurugan, S. Natarajan, *Dalton Trans.* **2004**, 2923–2928; b) D. L. Long, A. J. Blake, N. R. Champness, C. Wilson, M. Schroder, *Angew. Chem. Int. Ed.* **2001**, *40*, 2443–2447; c) Y. Wan, L. Jin, K. Wang, L. Zhang, X. Zheng, S. Lu, *New J. Chem.* **2002**, *26*, 1590–1596; d) B. D. Alleyne, A. R. Williams, L. A. Hall, *Inorg. Chem.* **2001**, *40*, 1045–1051; e) L. Pan, M. Zheng, Y. Wu, S. Han, R. Yang, X. Huang, J. Li, *Inorg. Chem.* **2001**, *40*, 828–830.
[8] M. Z. Yates, K. C. Ott, E. R. Birnbaum, T. M. McCleskey, *Angew. Chem.* **2002**, *114*, 494–496; *Angew. Chem. Int. Ed.* **2002**, *41*, 476–478.
[9] a) R. Yan, X. Sun, X. Wang, Q. Peng, Y. Li, *Chem. Eur. J.* **2005**, *11*, 2183–2195; b) Y. P. Fang, A. W. Xu, R. Q. Song, H. X. Zhang, L. P. You, J. C. Yu, H. Q. Liu, *J. Am. Chem. Soc.* **2003**, *125*, 16025–16034.
[10] a) F. Serpaggi, G. Férey, *J. Mater. Chem.* **1998**, *8*, 2749–2755; b) F. Serpaggi, G. Férey, *Inorg. Chem.* **1999**, *38*, 4741–4744.
[11] C. Tang, Y. Bando, D. Golberg, R. Ma, *Angew. Chem. Int. Ed.* **2005**, *44*, 576–579.
[12] a) D. Matsuura, *Appl. Phys. Lett.* **2002**, *81*, 4526–4529; b) G. Yi, B. Sun, F. Yang, D. Chen, Y. Zhou, J. Cheng, *Chem. Mater.* **2002**, *14*, 2910–2914; c) J. A. Cabobianco, J. C. Boyer, F.

Vetrone, A. Speghini, M. Bettinelli, *Chem. Mater.* **2002**, *14*, 2915–2921; d) A. Amitava, C. S. Friend, R. Kapoor, P. N. Prasad, *J. Phys. Chem. B* **2002**, *106*, 1909–1912.
[13] a) F. V. D. Rijke, H. Zijlmans, S. Li, T. Vail, K. A. Raap, R. S. Niedbala, H. J. Tanke, *Nat. Biotechnol.* **2001**, *19*, 273–276; b) J. Hampl, M. Hall, N. A. Mufti, Y. M. Yao, D. B. Macquee, W. H. Wright, D. E. Cooper, *Anal. Biochem.* **2001**, *288*, 176–187.
[14] W. C. W. Chan, S. M. Nie, *Science* **1998**, *281*, 2013–2016.
[15] M. Eddaoudi, H. L. Li, O. M. Yaghi, *J. Am. Chem. Soc.* **2000**, *122*, 1391–1397.
[16] a) K. L. Frindell, M. H. Bartl, A. Popitsch, G. D. Stucky, *Angew. Chem.* **2002**, *114*, 1001–1004; *Angew. Chem. Int. Ed.* **2002**, *41*, 959–962; b) M. Yada, M. Mihara, S. Mouri, M. Kuroki, T. Kijima, *Adv. Mater.* **2002**, *14*, 309–313; c) M. Yada, H. Kitamura, A. Ichinose, M. Machida, T. Kijima, *Angew. Chem.* **1999**, *111*, 3716–3720; *Angew. Chem. Int. Ed.* **1999**, *38*, 3506–3510.
[17] P. M. de Wolff, *J. Appl. Crystallogr.* **1968**, *1*, 108–113.
[18] G. S. Smith, R. L. Snyder, *J. Appl. Crystallogr.* **1979**, *12*, 60–65.
[19] P.-E. Werner, L. Eriksson, M. Westdahl, *J. Appl. Crystallogr.* **1985**, *18*, 367–370.
[20] a) C. T. M. Ribeiro, A. R. Zanatta, L. A. O. Nunes, *J. Appl. Phys.* **1998**, *83*, 2256–2261; b) J. A. Capobianco, F. Vetrone, T. D. Alesio, G. Tessari, A. Speghini, M. Bettinelli, *Phys. Chem. Chem. Phys.* **2000**, *2*, 3203–3207.
[21] G. Yi, B. Sun, F. Yang, D. Chen, Y. Zhou, J. Cheng, *Chem. Mater.* **2002**, *14*, 2910–2914.

Received: September 16, 2007
Published Online: March 17, 2008

